

Chapter

CMOS Compatible Wet Bulk Micromachining for MEMS Applications

S. Santosh Kumar and Ravindra Mukhiya

Abstract

Wet bulk micromachining of silicon is a convenient and economical method for realizing various silicon-based microsensors and actuators. Tetramethylammonium hydroxide (TMAH) based anisotropic wet etching is popular due to it being less toxic and CMOS compatible. The etch rate of TMAH depends on the wafer's crystal plane orientation and temperature/concentration of solution. While using TMAH to realize a pressure sensor diaphragm, the etching of {111} planes causes underetching, causing a deviation in the intended size of the diaphragm, inducing variation in the designed characteristics of the device. It is necessary to estimate and minimize these deviations. Experiments were designed and the rate of etching for (100) and (111) planes using 25 wt.% TMAH have been determined at different temperatures. Linear fit equations are obtained from experimental data to relate the underetch per unit depth to the solution temperature. These findings are extremely useful in the fabrication of silicon diaphragms with precise dimensions. While using anisotropic wet etchants to realize proof mass for accelerometers, the etchants attack the convex corners. This necessitates a suitable design of compensating structure while realizing microstructures with sharp convex corners. Experimental studies are carried out to protect convex corners from undercutting and the results are reported.

Keywords: TMAH etching, piezoresistive pressure sensor, diaphragm, underetching, convex corner compensation

1. Introduction

The process of bulk micromachining is carried out in order to etch out a significant portion of silicon from silicon substrate resulting in structures created out of silicon for different applications. Some of these structures include: diaphragms (for pressure sensors) [1], proof-mass (for accelerometers) [2], nozzle (for inkjet printer) [3], random pyramids on Si surface (for solar cells) [4], and cantilevers [5]. Aqueous TMAH is often used for realization of structures in silicon using wet anisotropic bulk micromachining. It offers an attractive low-cost alternative to dry bulk micromachining technique, which uses gases and expensive equipment. TMAH is favoured choice over other alternatives like KOH, EDP etc. for wet anisotropic etching due to complementary metal-oxide-semiconductor (CMOS) compatibility and less toxicity.

In industrial microelectronics process line or CMOS-MEMS processes, it is preferable to replace KOH with TMAH, to avoid contamination due to Potassium (K^+) ions. However, owing to a high undercutting ratio of TMAH, it entails a dedicated study on compensation structures. This has inspired us to carry out experimental studies using TMAH.

TMAH etching rate is generally governed by: the orientation of the Si wafer, the temperature of aq. TMAH solution and the TMAH concentration in aqueous solution [6]. Although TMAH etches aluminium when it comes in contact with it, it is possible to carry out post CMOS bulk micromachining with aluminium metallization using TMAH by dissolving silicon and oxidizers like ammonium peroxodisulphate into the solution [7, 8].

The undercutting of convex corners and non (111) planes in Si is helpful in realization of freely suspended microstructures using wet anisotropic etchants [9, 10]. However, when mesa type structures having convex corners are desired, these effect of undercutting of convex corners have to be checked and avoided, if possible. It has been observed that TMAH shows a high undercutting ratio in comparison to KOH. In this chapter, experimental studies and analysis to protect convex corners and non {111} crystal planes from undercutting during TMAH etching is described.

In this chapter, we present the studies related to realization of diaphragm (for piezoresistive pressure sensor) and proof-mass (for accelerometer) using aq. 25 wt. % TMAH solution. The importance of precise etching of diaphragm in piezoresistive pressure sensor is discussed in Section 2. Experimental evaluation of TMAH etching is carried out to determine the etch rate in (100) and (111) planes of silicon at different temperatures and is discussed in Section 3. The underetching of silicon diaphragm during TMAH etching is also determined to design proper dimensions of openings in mask sets. Corner compensation structures for TMAH, experimental details, and design analysis and discussion are presented in Sections 4–6, respectively.

2. Piezoresistive pressure sensor

Usually, a piezoresistive pressure sensor has four piezoresistors on a silicon diaphragm, close to the edges of the diaphragm, connected in a Wheatstone configuration. When the diaphragm is subjected to a pressure load, the deflection of the diaphragm leads to stress generation on the diaphragm. As the piezoresistors are placed near the surface of the diaphragm, they experience these stresses, leading to a change in the resistance of the piezoresistors. Prior to fabricating the sensor, the placement of piezoresistors on the diaphragm is optimized using finite element method (FEM) based tools.

Diaphragm in (100) silicon can be fabricated using TMAH by exploiting its anisotropic etching property. TMAH etches different silicon planes with different etch rates but it has a high etch rate in $\langle 100 \rangle$ direction. Subsequent to the groundbreaking paper by Tabata et al. [11], much research has been dedicated to analyse the etch rate of silicon for different crystallographic directions [6, 12, 13]. While realizing diaphragms using aq. TMAH etching in (100) silicon wafers, the expected position of the piezoresistors (determined using FEM based design simulations) may shift due to etching in {111} planes. This leads to the phenomenon of underetching, where the TMAH etches under the etching mask in a (100) wafer. Underetching may cause the piezoresistors to be shifted from their pre-planned position on the diaphragm, as shown in **Figure 1**. This induces variation in the designed characteristics of the device. Therefore, it is necessary to estimate and

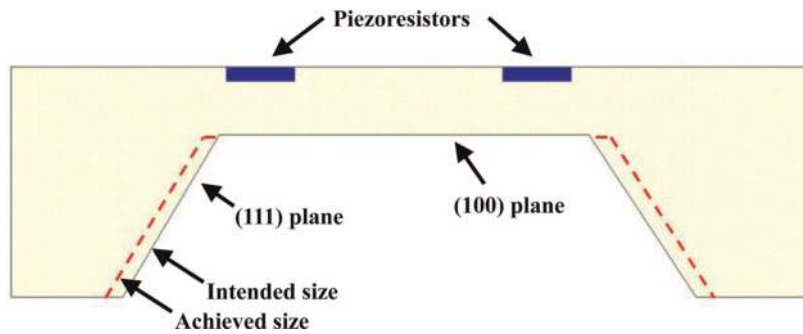


Figure 1. Cross-section of diaphragm of pressure sensor showing the displacement of position of piezoresistors due to etching by TMAH in $\{111\}$ planes.

minimize the deviation, especially in square diaphragms, where precise placement of piezoresistors is of prime importance for optimum performance of the device.

3. Experimental evaluation of TMAH etching for pressure sensor diaphragm

For the purpose of this study, experiments are designed and the etch rates in the $\{100\}$ and $\{111\}$ planes for 25 wt.% TMAH have been determined at different temperatures. Through these experiments, the underetching per unit depth of etching is also determined. This data can be used for selection of proper dimensions (based on the selected temperature of etching during fabrication) in the mask sets, compensating for the change in dimensions caused due to underetching. This method will ensure that diaphragms with accurate dimension are realized after etching.

The cross-section of the etch profile obtained during etching, while fabricating diaphragm structures on $\{100\}$ Si substrate using TMAH is shown in **Figure 2**. The figure distinctly depicts anisotropic etching by TMAH and also shows the underetching below the mask due to etching in $\{111\}$ planes. Alternatively, we can

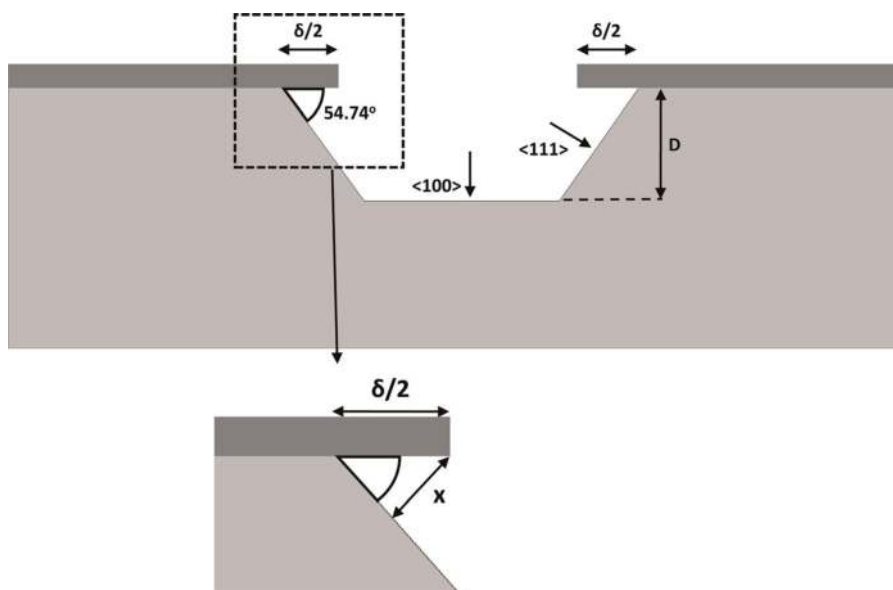


Figure 2. TMAH etch profile depicting etching in $\{100\}$ and $\{111\}$ planes.

also say that underetching is dependent on etch rate of TMAH in <110> direction. If we consider etching for time t , the <100> direction etch rate (ER) can be calculated by determining the etch depth (D) and dividing it by t . The <111> direction etch rate (x/t) can be calculated by determining the underetching ($\delta/2$) in the mask and subsequently applying the formulas as shown in Eqs. (1)–(3) [14].

$$\frac{x}{\delta/2} = \sin 54.74 = \frac{\sqrt{2}}{\sqrt{3}}, \delta = \sqrt{6}x \quad (1)$$

$$\text{ER of } \{111\} \text{ planes : } \frac{x}{t} = \frac{\delta}{\sqrt{6}t}, t = \text{etch time} \quad (2)$$

$$\text{Underetch per unit depth : } \frac{\delta/2}{D} \quad (3)$$

To ascertain the nature of etching in 25 wt.% aq. TMAH for (100) silicon at different temperatures, (100) Si n-type wafers with resistivity values in the range of 5–7 Ω -cm and a thickness of $527 \pm 2 \mu\text{m}$ are selected. Subsequently, a thermal SiO₂ layer of 1 μm thickness is grown (and afterward patterned) for use as masking layer. A single level mask is used to obtain the required diaphragms. The diaphragms etched using TMAH are then analyzed for feature dimensions to determine the (111) and (100) planes etch rates. Each sample was etched in TMAH at different temperature (with an accuracy of $\pm 1^\circ\text{C}$). For maintaining a constant concentration of TMAH in the aqueous solution, during the course of the experiment, suitable amount of deionized (DI) water was added after each experiment [15]. The etching on each sample was performed for 5 h. Six samples were used for six different temperatures.

The depth of the cavity (behind the diaphragm) for different samples is determined using a surface contact profilometer. The measured value is used to obtain the <100> direction etch rate. To obtain the <111> direction etch rate for different samples, the initial and final sizes of the square alignment mark are compared. The initial size of alignment mark would be equal to the size of cavity opening in the mask set. This determines the underetching by determining the length of hanging oxide. These measurements are carried out using scanning electron microscope (SEM). The underetch ($\delta/2$) obtained from SEM is used to calculate the <111> direction etch rate. A sample SEM image of the alignment marks, overall diaphragm and zoomed view of hanging oxide are shown in **Figures 3** and **4a** and **b** respectively. The experiments are performed for six temperatures. The computed <100> and <111> direction etch rates are listed in **Table 1**.

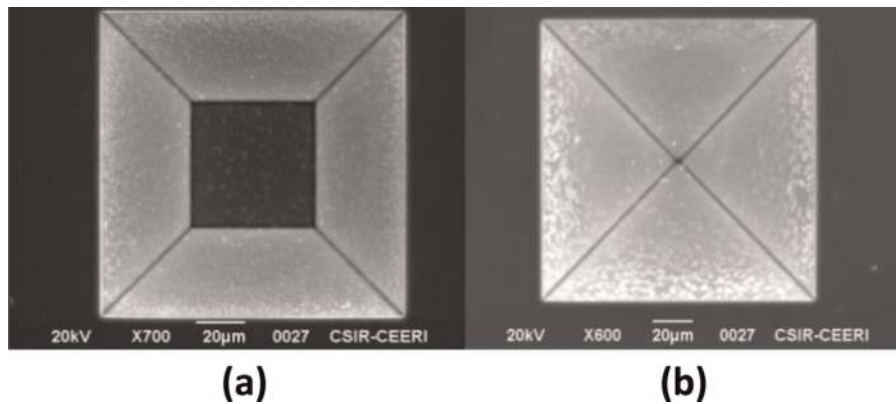


Figure 3. SEM image of alignment marks used for calculating underetching (a) alignment mark during etching and (b) alignment mark converted to V-groove.

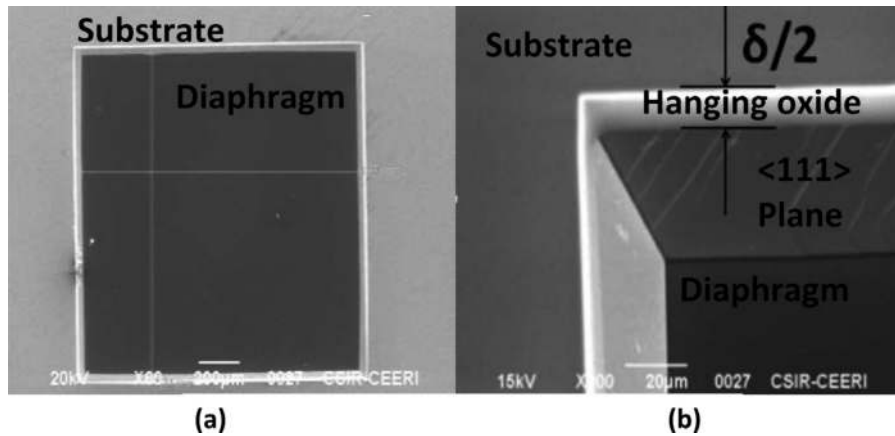


Figure 4. (a) SEM image of a diaphragm and (b) hanging oxide after TMAH etching [14] copyright 2014 by springer nature (used with permission).

| Solution temperature (°C) error = ±1 | Etch rate in <100> (μm/h) | Etch rate in <111> (μm/h) | Etch rate ratio <100>/<111> | Underetch per unit depth |
|--------------------------------------|---------------------------|---------------------------|-----------------------------|--------------------------|
| 63 | 10.02 | 1.15 | 8.71 | 0.141 |
| 68 | 13.80 | 1.29 | 10.69 | 0.114 |
| 73 | 17.98 | 1.40 | 12.84 | 0.095 |
| 78 | 21.62 | 1.73 | 12.49 | 0.098 |
| 83 | 30.38 | 1.89 | 16.07 | 0.076 |
| 88 | 38.90 | 2.00 | 19.45 | 0.063 |

Table 1. Etch rates of Si in TMAH [14]. Copyright 2014 by springer nature (used with permission).

It is evident from the table that the rate of etching increases both in the <100> and <111> direction with increase in temperature. The underetch per unit depth is determined by the ratio of etching in <110> direction to etching in <100> direction. It can be observed that the underetch per unit depth decreases with increased temperature. Alternatively stated, for the same etch depth in <100> direction, lesser underetching is obtained at higher temperatures. A minor deviation in this upward trend is observed between temperature of 73 and 78°C. This may be attributed to some error in experimentally observed data due to temperature variation in the TMAH solution. It may also be attributed to error in the measurement of the diaphragm size from SEM images. The plot of etch rate in <100> direction and underetch per unit depth with solution temperature is shown in **Figures 5 and 6**, respectively.

Based on the above observations, the following empirical equations (linear fit) are proposed for the etching rates in <100> and <111> direction in 25% wt. aq. TMAH at different temperatures:

$$\text{<100>etch rate} = 1.13 \times T - 63.21 \quad (4)$$

$$\text{<111>etch rate} = 0.0365 \times T - 1.176 \quad (5)$$

A new empirical linear fit equation is obtained from the data in **Table 1** to relate the underetch per unit depth of etching in (100) plane to the solution temperature, which is given by Eq. (6):

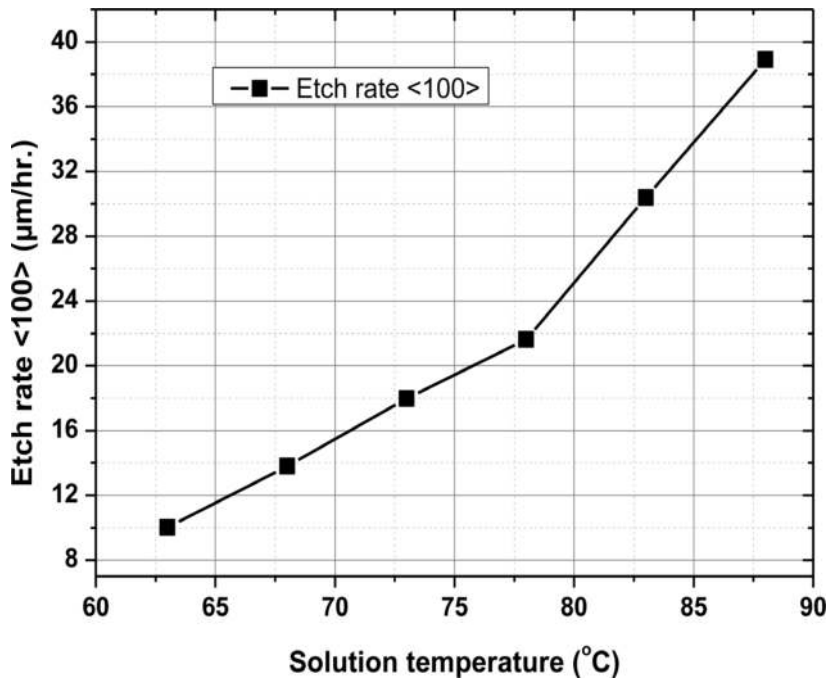


Figure 5.
Plot of etch rate in (100) plane vs. solution temperature.

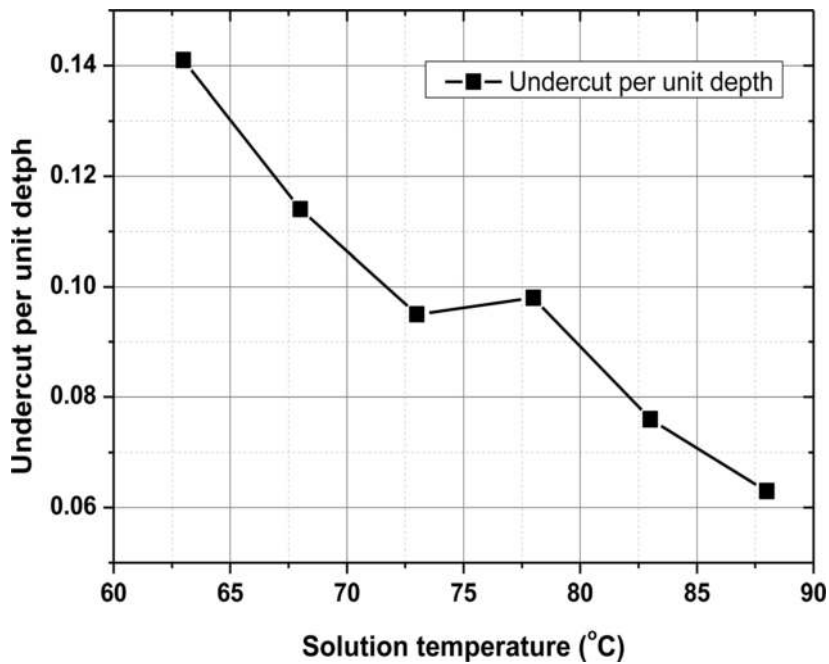


Figure 6.
Plot of underetch per unit depth vs. solution temperature.

$$\text{Underetch per unit depth} = 0.31398 - 0.00286 \times T \quad (6)$$

where T is the solution temperature.

This expression can be used to estimate the dimensions of the masks to be used for obtaining patterns using TMAH etching during fabrication of the pressure sensor. This study provides an important guideline towards making silicon diaphragms with precise dimensional control. Also, the study indicates that in the case

of mask sets which have been fabricated without considering the effect of underetching, a higher temperature must be used to minimize the effect of underetching on diaphragm dimensions.

4. Corner compensation structures for TMAH

In many applications of silicon microsensor/actuator structures, like accelerometer and bossed diaphragm pressure sensors, it is desired to have truncated pyramid or mesa type of structures to be realized and/or integrated with thin membrane or beams. During the wet chemical anisotropic etching, it is observed that the convex corners of mesa type structures deteriorates very fast and results in undesired shape/structure. This deterioration is mainly due to the fact that different crystal planes intercept at the convex corner and some of the planes are fast etching planes [10, 16]. The fast etching planes dominate over other crystal planes and hence results in the deterioration of the convex corner shape. This phenomenon is referred to as convex corner undercutting. In sensors structures, like accelerometer, it is needed to preserve the shape of mesas/truncated pyramid. These convex corners can be preserved by adding extra structures (known as convex corner compensation structures) at these convex corners, which are removed or etched out during the process of etching.

Some of the most common corner compensation structures are $\langle 110 \rangle$ square, $\langle 100 \rangle$ bar type (thin and wide bar structures) and triangle shape structures [17–23]. These compensation structures are shown in **Figure 7**, along with design parameters. Square compensation structures have edges aligned to $\langle 110 \rangle$ wafer flat direction is attached to one of the convex corners. Two kinds of bar structures (thin bar and wide bar or bar1 and bar2), aligned in $\langle 100 \rangle$ direction, are shown on

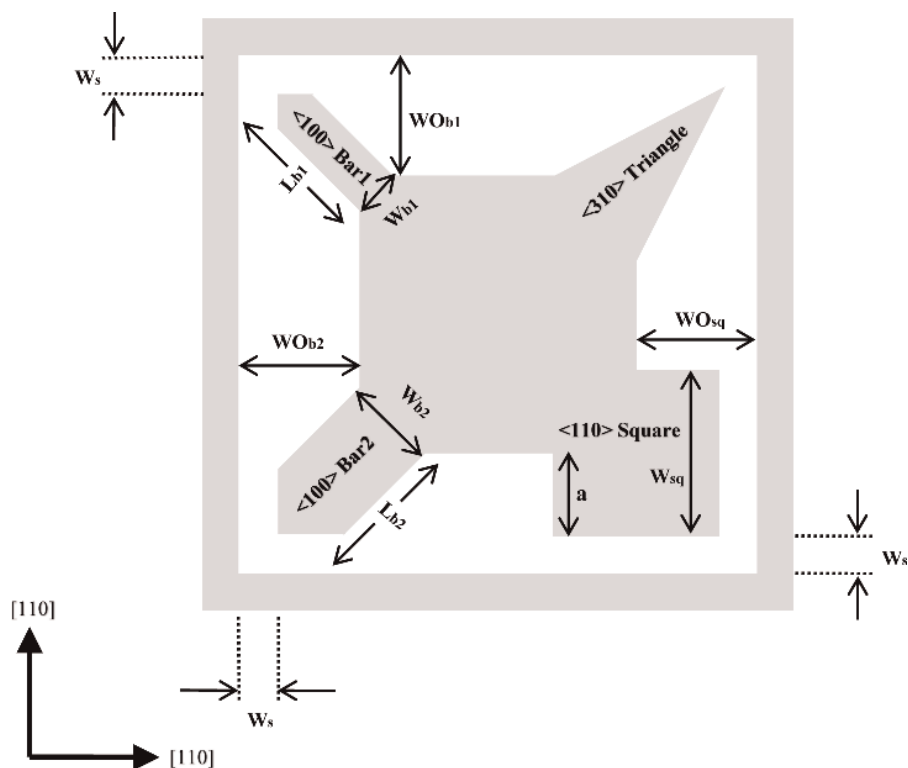


Figure 7.
Corner compensation structures.

two other corners. The convex corner, while the $\langle 310 \rangle$ triangle corner compensation structure is shown at the fourth corner. Design parameters and equations of the structures are discussed further in the chapter. In this chapter, we have focused only on $\langle 100 \rangle$ bar type structures because these are the ones which can give perfect convex corners with less space. The other structures are reported elsewhere [15].

5. Experimental details

Etch profile or undercutting of the convex corners depends on the crystallographic orientation of the wafer, alignment of structure pattern with the crystallographic direction, type of dopant and its concentration, type of etchant/chemical, chemical concentration, and temperature. We have performed experiments with silicon (100) substrate using 25 wt.% TMAH water solution at $90 \pm 1^\circ\text{C}$ temperature in a constant temperature bath. The details of experiment parameters are given in **Table 2**. Thermally grown silicon dioxide has compressive residual stress of ~ 100 MPa, which gives better adhesion and reduces the shape deterioration near the mask [24]. After carrying out thermal oxidation $\sim 1 \mu\text{m}$, the mask structures, with different compensating structures as shown in **Figure 7**, were transferred to the silicon substrate with its primary flat aligned with $\langle 110 \rangle$ and experiments were performed.

To understand the etch profile and morphology, the samples were removed from the bath, cleaned and examined periodically. Depth was measured using a digital microscope with an accuracy of $\pm 2 \mu\text{m}$. It was observed that the profile is consistent in repeated experiments and has a front etch angle of $\sim 25^\circ$, which corresponds to the $\{311\}$ planes and $[310]$ directions. A square mask aligned to $\langle 110 \rangle$ direction without any compensation structure was used to measure the front etch attack angle. The measured data agrees with the reported literature [25, 26]. In KOH $\{411\}$ planes are responsible for convex corner undercutting [17], while in TMAH $\{311\}$ planes are responsible [25, 26].

| Parameters | Value |
|-----------------------------|---|
| Substrate and size | Silicon, 4-in. |
| Orientation | (100) |
| Type and dopant | n-type, phosphorus |
| Resistivity | 8–10 $\Omega\text{-cm}$ |
| Structure alignment | $\langle 110 \rangle$ direction |
| Substrate thickness | $\sim 525 \mu\text{m}$ |
| Masking layer and thickness | Silicon dioxide, $\sim 1 \mu\text{m}$ (thermally grown) |
| Etchant | 25 wt.% TMAHW |
| Temperature | $90 \pm 1^\circ\text{C}$ |
| Stirring | No |
| Etch front angle | 24–25° |
| Fast etch plane | $\{311\}$ |
| Fast etch direction | $\langle 310 \rangle$ |

Table 2. Silicon substrate specifications and etching parameters [23].

From the experiments the etching parameters were extracted and summarized in **Table 3**, along with compensating structure dimensions.

5.1 <100> thin bar structure etching mechanism

<100> thin bar (structure 1) is longer and has less width. This structure has etching in two sides in <100> direction and from front side in <310> direction. In <100> direction the etching is similar to the (100) plane and in front side it is faster due to fast etch plane {311}. In this compensation structure, the depth is controlled by the width of the bar (twice of the etch depth) and the convex corner shape is preserved by front of the beam. The length should be more than the width. Thus, the convex shape is preserved completely. The convex corner of the final structure obtained by bar1 compensation structure is shown in **Figure 8**.

5.2 <100> wide bar structure etching mechanism

<100> wide bar (structure 2) is shorter in length and wider in width. This structure has also etching in two sides in <100> direction and from front side in <310> direction. In <100> direction the etching is similar to the (100) plane and in front side it is faster due to fast etch plane {311}. In this compensation structure, the depth is controlled by the length of the bar and the convex corner shape is preserved by {310} etch front of the beam. By increasing the width, requirement of the length is reduced. Thus, the convex shape is preserved completely. The convex corner of the final structure obtained by bar2 compensation structure is shown in **Figure 9**.

| Parameters | Value |
|---|---|
| (100) plane etch rate: ER (100) | 0.67 $\mu\text{m}/\text{min}$ |
| (111) plane etch rate: ER (111) | 0.048 $\mu\text{m}/\text{min}$ |
| (311) plane etch rate: ER (311) | 1.494 $\mu\text{m}/\text{min}$ |
| Anisotropic ratio: ER (111)/ER (100) | 0.071 |
| Anisotropic ratio: ER (311)/ER (100) | 2.23 |
| Minimum side separation: Ws | 10 μm (for all the structures) |
| <100> thin bar structure design dimensions: | |
| <100> thin bar width: Wb1 | 860 μm |
| <100> thin bar length: Lb1 | 1918 μm |
| <100> thin bar minimum window opening: WOb1 | 1366 μm |
| Alignment angle with <110> primary flat | 45° |
| <100> wide bar structure design dimensions: | |
| <100> thin bar width: Wb2 | 1802 μm |
| <100> thin bar length: Lb2 | 1499 μm |
| <100> thin bar minimum window opening: WOb2 | 1070 μm |
| Alignment angle with <110> primary flat | 45° |

Table 3. Etch rate parameters and compensating structure dimensions [23].

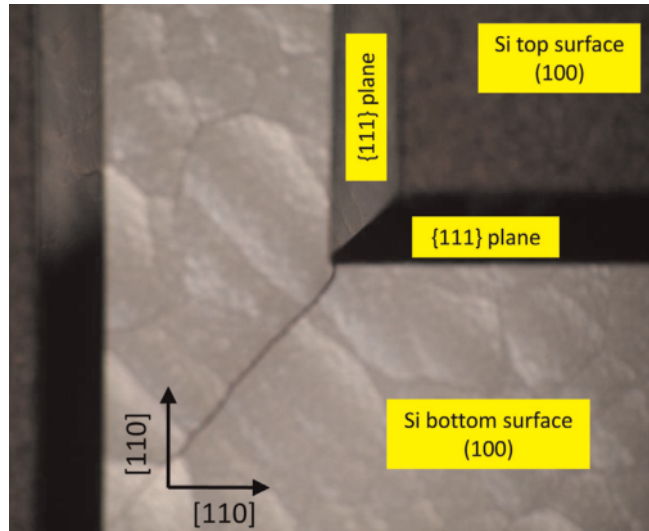


Figure 8.
Optical photograph of the convex corner realized using the $\langle 100 \rangle$ thin bar. [23] Copyright 2006 by IOP Publishing Ltd. (used with permission).

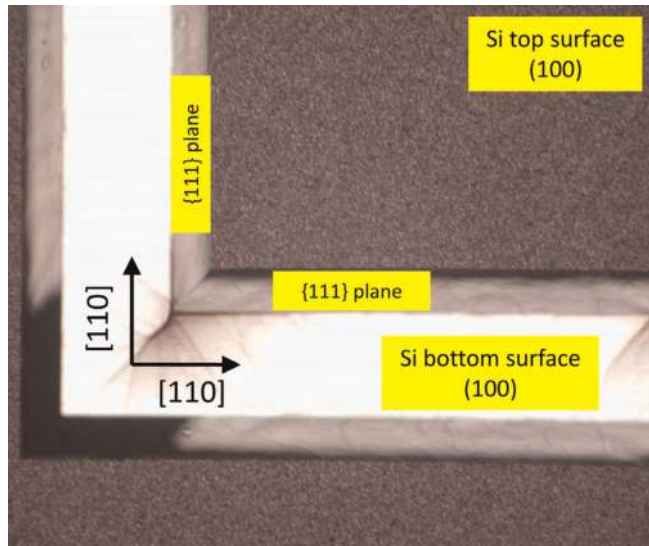


Figure 9.
Optical photograph of the convex corner realized using the $\langle 100 \rangle$ wide bar. [23] Copyright 2006 by IOP Publishing Ltd. (used with permission).

6. Design analysis and discussions

Optical photographs of the realized convex corners using the $\langle 100 \rangle$ thin and wide bars are depicted in **Figures 8** and **9**. As shown in **Figure 8**, for the dimensions mentioned earlier, a perfect convex corner is obtained for the $\langle 100 \rangle$ thin bar with free end at a depth of etching equal to $430 \mu\text{m}$. As shown in **Figure 9**, for the dimensions mentioned earlier, a perfect convex corner is obtained for the $\langle 100 \rangle$ wide bar at a depth of etching equal to $485 \mu\text{m}$. The thin bar is narrower in terms of width and longer in terms of length than the wide bar structure.

We can infer from **Figures 8** and **9** that perfect convex corners are obtained in each of the compensation structures—wide bar and thin bar. Bar2 requires less window opening compared to bar1. On the basis of the examination of the

experimental results, equations to design these structures are deduced and reported in Mukhiya et al. [23]. For bar1 structure, design is given by Eqs. (7) and (8), as follows [23]:

$$W_{b1} = 2D_e \quad (7)$$

$$WO_{b1} = W_s + 1.414 \frac{R(311)}{R(100)} D_e \quad (8)$$

For bar2 structure, design is given by Eqs. (9) and (10), as follows [23]:

$$W_{b2} \leq \left[2.07 \frac{R(311)}{R(100)} - 0.336 \right] D_e \quad (9)$$

$$WO_{b2} \geq W_s + \left[0.351 + 0.734 \frac{R(311)}{R(100)} \right] D_e \quad (10)$$

where D_e is the etch depth. The remaining symbols have been defined earlier in the chapter. In order to obtain perfect convex corners for the bar structures, Eqs. (7)–(10) provide the biggest and smallest dimensions of width of beam and window opening, respectively.

From etch profile of both the $\langle 100 \rangle$ bar compensation structures, it is observed that they self-align with the $[310]$ direction, which is the fastest etch plane direction. Compensating structure designed with $[310]$ triangle shape will have consistent etch profile but it will require more space. Bar2 structure is $\sim 37\%$ more space efficient as compared to bar1 for the same etch depth.

7. Conclusions

With the advancement of technology, it is preferred to have CMOS-MEMS integration. This imposes the challenge of development of CMOS compatible processes and micromachining techniques. Among various micromachining techniques, wet bulk micromachining is a preferred technique because it is easy, cost-effective and has well defined characteristics. In spite of extensive research in this field, wet bulk micromachining using TMAH is still an interesting area of research among the researchers and academicians. Post process CMOS compatible wet bulk micromachining is possible with TMAH. By adding some additives, it is also possible to protect Aluminum in TMAH-based etchants. In the presented work, etch rates for different crystal planes have been measured at various temperatures. It is observed that for 25 wt.% TMAH underetching of $\{111\}$ planes increase with increase in temperature. However, the anisotropy ratio (111/100) decreases with temperature. Etch rate of both the crystal planes, (100) and (111), increases with temperature, as bond becomes weak at higher temperature. Etch rate of (100) plane is faster than the etch rate of (111) because (100) is a low atomic density plane. Empirical design equations have been derived for the etch rates as a function of temperature. As a use case of this anisotropic etching, diaphragm of pressure sensor has been fabricated at the authors' laboratory and its analysis in context of TMAH etching is presented.

It is observed that during wet anisotropic etching using 25 wt.% TMAH, the convex corners etches very fast and deteriorates in shape. This deterioration is known as undercutting, and it is mainly due to the fact that different crystal planes are encountered at the convex corner and some of the crystal planes etch very fast in comparison to other planes. These fast etching planes are responsible for the

undercutting. For TMAH, the fast etching planes are found at an angle of $\sim 25^\circ$, which are {311} plane. In case of TMAH, the underetching and undercutting are found faster than its counterpart KOH. In many applications, where these convex corners are required to be protected, some additional structures are added to protect the convex corner from deterioration. These are known as convex corner compensation structures. Most common compensation structure have been discussed and optimum structure, i.e., $\langle 100 \rangle$ bar type of structures (thin bar and wide bar) have been discussed in detail. Both the structures can protect the mesa and can give perfect convex corner. Bar2 structure is more space efficient than bar1 structure. Using this type of compensation structures, accelerometer proof mask has been fabricated at authors' laboratory and presented. Generalized empirical design equations have also been discussed.

Acknowledgements


Authors would like to acknowledge the generous support of the Director, CSIR-CEERI, Pilani. The authors would also like to thank all the scientific and technical members of Smart Sensors Area at CSIR-CEERI, Pilani. The financial support by CSIR, New Delhi to carry out the research work through various projects is gratefully acknowledged. R Mukhiya acknowledges FBK, Trento, Italy, for the experimental study on corner compensation structures, and DST for the financial support through the ITPAR project.

Author details

S. Santosh Kumar* and Ravindra Mukhiya
CSIR-Central Electronics Engineering Research Institute, Pilani, Rajasthan, India

*Address all correspondence to: santoshkumar.ceeri@gmail.com

IntechOpen

© 2019 The Author(s). Licensee IntechOpen. This chapter is distributed under the terms of the Creative Commons Attribution License (<http://creativecommons.org/licenses/by/3.0>), which permits unrestricted use, distribution, and reproduction in any medium, provided the original work is properly cited. 

References

- [1] Bhat KN. Silicon micromachined pressure sensors. *Journal of the Indian Institute of Science*. 2007;**87**(1): 115-131
- [2] Sharma A, Mukhiya R, Santosh Kumar S, Gopal R, Pant BD. Dynamic characterization of bulk micromachined accelerometer using laser doppler vibrometer (LDV). *Microsystem Technologies*. 2015;**21**:2221-2232. DOI: 10.1007/s00542-014-2316-3
- [3] Wei J, Sarro PM, Duc TC. A piezoresistive sensor for pressure monitoring at inkjet nozzle. In: *Proceedings of IEEE Sensors 2010*; 1-4 November 2010; USA, New York: IEEE; 2011. pp. 2093-2096
- [4] You JS, Kim DH, Huh JY, Park HJ, Pak JJ, Kang CS. Experiments on anisotropic etching of Si in TMAH. *Solar Energy Materials and Solar Cells*. 2001; **66**:37-44. DOI: 10.1016/S0927-0248(00)00156-2
- [5] Bashir R, Hilt JZ, Elibol O, Gupta A, Peppas NA. Micromechanical cantilever as an ultrasensitive pH microsensor. *Applied Physics Letters*. 2002;**81**(16): 3091-3093. DOI: 10.1063/1.1514825
- [6] Tokoro K, Uchikawa D, Shikida M, Sato K. Anisotropic etching properties of silicon in KOH and TMAH solutions. In: 25-28 Nov. 1998; Japan, New York: IEEE; 2002. pp. 65-70
- [7] Yan G-Z, Chan PCH, Hsing I-M, Sharma RK, Sin JKO. An improved Si-etching solution without attacking exposed aluminum. *Sensors and Actuators A*. 2001;**89**:135-141. DOI: 10.1109/MEMSYS.2000.838579
- [8] Fujitsuka N, Hamaguchi K, Funabashi H, Kawasaki E, Fukada T. Aluminum protected silicon anisotropic etching technique using TMAH with an oxidizing agent and dissolved Si. *R&D Review of Toyota CRDL*. 2004;**39**:34-40
- [9] Seidel H. The mechanism of anisotropic silicon etching and its relevance for micromachining. In: *Proc. Transducers '87, Rec. 4th Int. Conf. Solid-State Sensors and Actuators*; 2-5 June 1987; Tokyo: Japan; pp. 2093-2096
- [10] Koide, Sato K, Tanaka S. Simulation of two-dimensional etch profile of silicon during orientation-dependent anisotropic etching. In: *Proceedings of the IEEE Microelectromechanical Systems (MEMS) Workshop*; Nara: Japan; 1991. pp. 216-220
- [11] Tabata O, Asahi R, Funabashi H, Shimaoka K, Sugiyama S. Anisotropic etching of silicon in TMAH solutions. *Sensors and Actuators A*. 1992;**34**:51-57. DOI: 10.1016/0924-4247(92)80139-T
- [12] Pal P, Sato K, Gosalvez MA, Shikida M. Study of rounded concave and sharp edge convex corners undercutting in CMOS compatible anisotropic etchants. *Journal of Micromechanics and Microengineering*. 2007;**17**:2299-2307. DOI: 10.1088/0960-1317/17/11/017
- [13] Thong JTL, Choi WK, Chong CW. TMAH etching of silicon and the interaction of etching parameters. *Sensors and Actuators A*. 1997;**63**: 243-249. DOI: 10.1016/S0924-4247(97)80511-0
- [14] Santosh Kumar S, Pant BD. Design principles and considerations for the 'ideal' silicon piezoresistive pressure sensor: A focused review. *Microsystem Technologies*. 2014;**20**:1213-1247. DOI: 10.1007/s00542-014-2215-7
- [15] Mukhiya R, Bagolini A, Bhattacharyya TK, Lorenzelli L, Zen M. Experimental study and analysis of

corner compensation structures for CMOS compatible bulk micromachining using 25 wt.% TMAH. *Microelectronics Journal*. 2011;**42**:127-134. DOI: 10.1016/j.mejo.2010.08.018

[16] Offereins HL, Kühl K, Sandmaier H. Methods for fabrication of convex corners in anisotropic etching of (100) silicon in aqueous KOH. *Sensors and Actuators A*. 1990;**25**:9-13. DOI: 10.1016/0924-4247(90)87002-Z

[17] Mayer GK, Offereings HL, Sandmaier H, Kühl K. Fabrication of non-underetched convex corner in anisotropic etching of (100) silicon in aqueous KOH with respect to novel micromechanical elements. *Journal of the Electrochemical Society*. 1990;**137**: 3947-3951. DOI: 10.1149/1.2086334

[18] Enoksson P. New structure for corner compensation in anisotropic KOH etching. *Journal of Micromechanics and Microengineering*. 1997;**7**:141-144. DOI: 10.1088/0960-1317/7/3/016

[19] Zhang Q, Liu L, Li Z. A new approach to convex corner compensation for anisotropic etching of (100) Si in KOH. *Sensors and Actuators A*. 1996;**56**:251-254. DOI: 10.1016/S0924-4247(96)01312-X

[20] Puers B, Sansen W. Compensation structures for convex corner micromachining in silicon. *Sensors and Actuators A*. 1990;**23**:1036-1041. DOI: 10.1016/0924-4247(90)87085-W

[21] Bao M, Burrer C, Esteve J, Bausells J, Marco S. Etching front control of <110> strips for corner compensation. *Sensors and Actuators A*. 1993;**37-38**:727-732. DOI: 10.1016/0924-4247(93)80123-X

[22] Wu X-P, Ko WH. Compensating corner undercutting in anisotropic etching of (100) silicon. *Sensors and Actuators A*. 1989;**18**:207-215. DOI: 10.1016/0250-6874(89)87019-2

[23] Mukhiya R, Bagolini A, Margesin B, Zen M, Kal S. <100> bar corner compensation for CMOS compatible anisotropic TMAH etching. *Journal of Micromechanics and Microengineering*. 2006;**16**:2458-2462. DOI: 10.1088/0960-1317/16/11/029

[24] Takao H, Yong C-C, Rajanna K, Ishida M. Shape deterioration of mesa structures in post-CMOS anisotropic etching of silicon microstructures: An experimental study. *Sensors and Actuators A*. 2000;**86**:115-121. DOI: 10.1016/S0924-4247(00)00437-4

[25] Tellier CR, Charbonnieras AR. Characterization of the anisotropic chemical attack of (h h l) silicon plates in a TMAH 25 wt.% solution: Micromachining and adequacy of the dissolution slowness surface. *Sensors and Actuators A*. 2003;**105**:62-75. DOI: 10.1016/S0924-4247(03)00064-5

[26] Trieu HK, Mokwa W. A generalized model describing corner undercutting by the experimental analysis of TMAH/IPA. *Journal of Micromechanics and Microengineering*. 1998;**8**:80-83. DOI: 10.1088/0960-1317/8/2/009